

Detecting topological invariants in non-unitary discrete-time quantum walks

Xiang Zhan,¹ Lei Xiao,¹ Zhihao Bian,¹ Kunkun Wang,¹ Xingze Qiu,^{2,3} Barry C. Sanders,^{3,4,5,6} Wei Yi,^{2,3,*} and Peng Xue^{1,7,†}

¹Department of Physics, Southeast University, Nanjing 211189, China

²Key Laboratory of Quantum Information, University of Science and Technology of China, CAS, Hefei 230026, China

³Synergetic Innovation Center in Quantum Information and Quantum Physics, University of Science and Technology of China, CAS, Hefei 230026, China

⁴Hefei National Laboratory for Physical Sciences at Microscale, University of Science and Technology of China, CAS, Hefei 230026, China

⁵Institute for Quantum Science and Technology, University of Calgary, Alberta T2N 1N4, Canada

⁶Program in Quantum Information Science, Canadian Institute for Advanced Research, Toronto, Ontario M5G 1M1, Canada

⁷State Key Laboratory of Precision Spectroscopy, East China Normal University, Shanghai 200062, China

We report the experimental detection of bulk topological invariants in non-unitary discrete-time quantum walks with single photons. The non-unitarity of the quantum dynamics is enforced by periodically performing partial measurements on the polarization of the walker photon, which effectively introduces loss to the dynamics. The topological invariant of the non-unitary quantum walk is manifested in the quantized average displacement of the walker, which is probed by monitoring the photon loss. We confirm the topological properties of the system by observing localized edge states at the boundary of regions with different topological invariants. We further demonstrate the robustness of both the topological properties and the measurement scheme of the topological invariants against disorder.

PACS numbers: 03.67.Ac, 42.50.-p, 03.65.Vf, 42.50.Ar

Introduction:— Topological phases, with their remarkable properties, have been under intensive study in recent years [1, 2]. Besides condensed-matter materials such as topological insulators and superconductors, topological phenomena also emerge in synthetic systems ranging from classical light and microwaves transporting in periodically modulated media [3–16] and phononic states in mechanical oscillators [17, 18], to cold atoms in optical lattices [19–25] and photons in discrete-time quantum walks (QWs) [26]. A prominent feature of a topological phase is the emergence of topologically protected edge states, which are robust under symmetry-preserving perturbations and play a crucial role in the topological functionality of the underlying system. Through the so-called bulk-boundary correspondence, the existence and the number of these edge states are dictated by the integer-valued topological invariants, which are pivotal to the characterization of topological phases [27, 28]. While many experiments are concerned with the detection and characterization of topological edge states, recent progress has led to the direct measurement of topological invariants in the bulk of synthetic topological systems [9–12, 19, 21, 22, 29, 30]. The highly controllable parameters of these synthetic simulators offer the exciting possibility of extending the study of topological matter to regimes beyond the scope of conventional electronic systems in the condensed-matter setting.

An outstanding example here is the identification of topological phenomena in dissipative non-Hermitian systems [12, 13, 15, 31–34]. In particular, as predicted by Rudner and Levitov [31, 32], for a particle mov-

ing on a one-dimensional superlattice with losses on a given sublattice site in each unit cell, the average displacement of the particle is quantized, and is associated with a topological invariant defined in terms of the eigenstates of the non-Hermitian Hamiltonian. This new paradigm of topology is then experimentally confirmed in [12], where the quantized mean displacement of light propagating in a lossy optical waveguide array is measured and associated with topologically non-trivial properties. While the experimental system in [12] features continuous-time non-Hermitian dynamics, an important question is whether topological invariants can also be defined for discrete-time non-unitary dynamics. This is particularly interesting in light of the recent demonstration of topological properties in unitary discrete-time QWs [9, 10, 26, 29, 30].

In this work, we report the first experimental detection of bulk topological invariants in a non-unitary discrete-time QW using single photons. To exploit the quantum nature of single photons, we entangle the photonic walker with an ancillary photon, which allows the manipulation of the dynamics in a delayed-choice fashion [35, 36]. By periodically performing partial measurements on the photon polarization of the walker [37], we realize a non-unitary QW supporting Floquet topological phases (FTPs). While a given FTP typically features two distinct topological invariants [38–40], we demonstrate that both topological invariants can be detected from the average displacement of the walker. The topological properties of the quantum dynamics are confirmed by the observation of localized edge states at the bound-

ary between regions with distinct topological invariants. Finally, we demonstrate the robustness of the topological properties as well as the measurement scheme against disorder. Our work opens up the avenue of analyzing topological features in discrete-time quantum dynamics governed by non-unitary Floquet operators.

Non-unitary discrete-time QWs:— We start from a split-step QW governed by the unitary Floquet operator $U' = R(\frac{\theta_1}{2})SR(\theta_2)SR(\frac{\theta_1}{2})$. Here $R(\theta) = \mathbb{1}_w \otimes e^{-i\theta\sigma_y}$ is the coin operator rotating the coin state about the y -axis by θ , $\mathbb{1}_w = \sum_x |x\rangle\langle x|$, x denotes the position of the walker, $\sigma_y = i(|0\rangle\langle 1| - |1\rangle\langle 0|)$ is the standard Pauli operator, and $\{|0\rangle, |1\rangle\}$ are two orthogonal coin states. The position shift operator S is given by $S = \sum_x (|x-1\rangle\langle x| \otimes |0\rangle\langle 0| + |x+1\rangle\langle x| \otimes |1\rangle\langle 1|)$.

Non-unitary time-evolution is then enforced by performing the partial measurement $M_e = \mathbb{1}_w \otimes \sqrt{p}|- \rangle\langle -|$ at each time step, where $0 < p \leq 1$ is the probability of a successful (positive) measurement and $|\pm\rangle = (|0\rangle \pm |1\rangle)/\sqrt{2}$ [37]. When the walker is not detected, a negative measurement is applied and the state evolves as $|\psi_t\rangle = (\tilde{U}')^t |\psi_0\rangle$ after t steps, where $|\psi_0\rangle$ is the initial state of the walker-coin system, $\tilde{U}' = MU'$, and $M = \mathbb{1}_w \otimes (|+\rangle\langle +| + \sqrt{1-p}|- \rangle\langle -|)$. The probability of the walker being detected at x during the t -th step is $P_{\text{th}}(x, t) = \langle \psi_{t-1} | U'^{\dagger} M_e^{\dagger} (|x\rangle\langle x| \otimes \mathbb{1}_c) M_e U' | \psi_{t-1} \rangle$, where $\mathbb{1}_c$ is a 2×2 identity operator.

Interestingly, FTPs emerge in the non-unitary QW dynamics above, which can be understood by introducing the effective Hamiltonian defined through $\tilde{U}' = \exp(-iH_{\text{eff}})$. In momentum space, we have $H_{\text{eff}}(k) = E_k \mathbf{n} \cdot \boldsymbol{\sigma}$, with $\boldsymbol{\sigma}$ the Pauli vector and \mathbf{n} the direction of the spinor eigenstate at each momentum $-\pi < k \leq \pi$. In the limit of $p = 0$, we have $M = \mathbb{1}_w \otimes \mathbb{1}_c$, and the corresponding unitary discrete-time QW features a FTP protected by chiral symmetry [26, 41]. The topological invariant in this case is given by the so-called winding number, i.e., the number of times the vector \mathbf{n} , which lies in the y - z plane, winds around the x -axis as k varies through the first Brillouin zone [41]. For $p > 0$, the time-evolution becomes non-unitary, and \mathbf{n} is no longer a real vector lying in the y - z plane. However, as we show in the Supplemental Materials, one can still define the winding number here as the number of times the real components of \mathbf{n} winds around the x -axis as k varies through the first Brillouin zone [12, 32, 36]. Notably, for a given FTP, typically two distinct winding numbers (ν' , ν'') exist for Floquet operators fitted in different time frames [40]. While the corresponding winding number for \tilde{U}' is ν' , ν'' is associated with $\tilde{U}'' = MR(\frac{\theta_2}{2})SR(\theta_1)SR(\frac{\theta_2}{2})$. Alternatively, one may define the topological invariants $(\nu_0, \nu_\pi) = [(\nu' + \nu'')/2, (\nu' - \nu'')/2]$, which are related to edge states at the boundaries through the bulk-boundary correspondence for Floquet systems [36, 40]. In Fig. 1(a), we show the phase diagram on the θ_1 - θ_2 plane with both

sets of topological invariants.

Similar to the continuous-time non-Hermitian dynamics, the topological invariants of the discrete-time non-unitary QW can be detected by measuring the average displacement of the walker initially prepared in the non-loss state $|+\rangle$ at $x = 0$ [37]. Here the average displacement is given by $\langle \Delta x \rangle = \sum_x \sum_{t'=1}^{\infty} x P_{\text{th}}(x, t')$. The average dwell time, which characterizes the expected lifetime of the walker before it is measured and lost, is defined as $\langle t \rangle = \sum_x \sum_{t'=1}^{\infty} t' P_{\text{th}}(x, t')$.

Experimental Realization of non-unitary QWs:— As illustrated in Fig. 1(b), we implement delayed-choice QWs of single photons entangled with ancillary photons, which are subject to delayed-choice coin-state projections [35]. The coin states are represented by the horizontal $|H\rangle$ and vertical $|V\rangle$ polarization states of the photons, and the walker states are encoded in their spatial modes.

For the initial state preparation, the photon pairs are generated via type-I spontaneous parametric downconversion in a Bell state $|\Phi^+\rangle = (|HH\rangle + |VV\rangle)/\sqrt{2}$. One photon serves as a trigger and is projected in $|+\rangle$ with a half-wave plate (HWP) and a polarizing beamsplitter (PBS). The other photon is delayed-chosen to be the initial coin state $|+\rangle$ heralded by the trigger photon and then sent to the QW interferometric setup. The two-photon polarization entanglement is characterized using state tomography, with the visibility $> 95\%$ for $|\Phi^+\rangle$.

The coin operator is implemented by two HWPs with certain setting angles depending on the coin parameters (θ_1, θ_2) . The shift operator S is implemented via a birefringent beam displacer (BD), so that the photons in $|V\rangle$ are directly transmitted and those in $|H\rangle$ undergo a lateral displacement into a neighboring mode.

The partial measurement operator M_e in each step can be realized by a sandwich-type setup involving two HWPs and a partially polarizing beamsplitter (PPBS) with the transmissivity of horizontally and vertically polarized photons $(T_H, T_V) = (1, 1-p)$. The PPBS fully transmits horizontally polarized photons, and partially reflects vertically polarized photons, which gives the required polarization-dependent photon loss. Two HWPs at 22.5° are used to rotate the polarization of photons (i.e., a Hadamard operation $|V\rangle\langle -| + |H\rangle\langle +|$ on the polarization states). Thus, photons in $|-\rangle$ are reflected by the PPBS with a probability p , and then detected by a single-photon avalanche photodiode (APD). The remaining photons continue the QW dynamics after another polarization rotation via the second HWP, until they are detected and lost from the system. For a t -step QW, we perform coincidence measurements on the reflected photons at each position successively up to t and obtain $N_R(x, t')$ ($t' = 1, \dots, t$). Together with the measurement on the number of transmitted photons $N_T(x, t)$ at the last step t , we construct the probability $P_{\text{exp}}(x, t) = N_R(x, t') / \sum_{x'} \left[\sum_{t''=1}^t N_R(x', t'') + N_T(x', t) \right]$, from

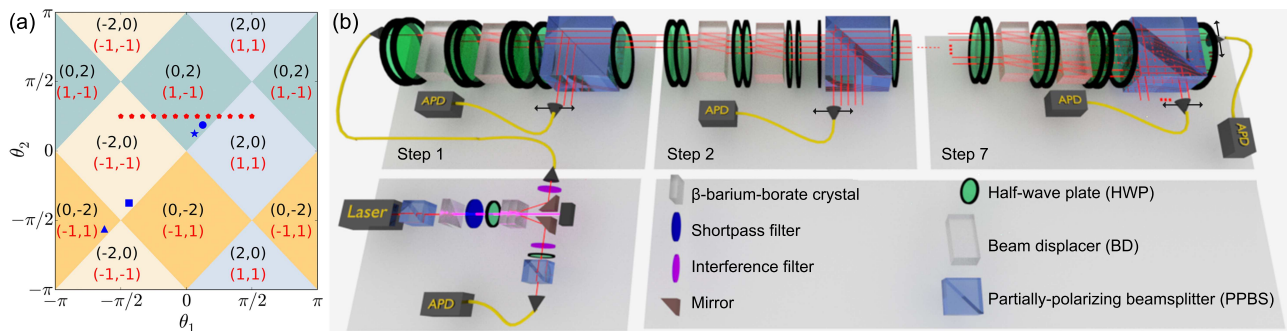


FIG. 1. (a) Phase diagram indicating the topological invariants (ν', ν'') (black) and (ν_0, ν_π) (red) as functions of the coin parameters (θ_1, θ_2) . The red dots indicate 13 sets of coin parameters used to detect the topological invariants. The blue dot indicates the parameters of inhomogeneous coin rotations for the inner region and the other blue symbols for the outer regions which are used to observe the topological edge states. (b) Experimental setup. The photon pair is created via spontaneous parametric downconversion in a Bell state $|\Phi^+\rangle$. One photon as a trigger is projected in the polarization state $|+\rangle$ with a HWP and a polarizing beamsplitter. The other photon undergoes QW interferometric network. The polarization rotation R and translation S can be realized by two HWPs with certain setting angles and a BD, respectively. The partial measurement via loss M_e is implemented by a sandwich-type HWP-PPBS-HWP setup. The photons appearing in the spatial modes at the output of a QW are coupled into optical fibers and then detected by APDs, in coincidence with the trigger photon. Photon counts are measured by translating the fiber coupler between the individual modes [42], which gives the measured probabilities after correcting for the relative efficiencies of the different APDs.

which the average displacement and dwell time are calculated.

We note that the partial measurement operator M_e is valid at the single-photon level. In our experiment, coincidence counts of up to 8000 have been observed with the source, where heralded single photons sharing entanglement with ancillary photons are used. The probability of a multi-photon event is negligibly small ($< 10^{-4}$). It is therefore reasonable to model the sandwich-type HWP-PPBS-HWP setup using M_e .

Detecting topological invariants:— We realize 7-step QWs with a fixed $\theta_2 = \pi/4$ and varying θ_1 , for different loss parameters $p = 1, 2/3, 9/25$. The walker starts from $x = 0$, and the initial coin state is chosen to be $|+\rangle$ via the delayed-choice setting. The measured average displacements are shown in Figs. 2(a) and (b) (upper layer) respectively for evolution operators \tilde{U}' and \tilde{U}'' . The results agree reasonably well with the numerical simulations of 7-step QWs and demonstrate plateaux close to the quantized values ν' and ν'' calculated from infinite-step QWs. Near topological phase transitions, where the topological invariants undergo abrupt changes, the measured average displacements deviate from the quantized topological invariants, as it takes more time for the average displacements to reach quantized values here. Such a feature can be confirmed by calculating the average dwell time of infinite-step QWs, which becomes divergent close to phase transitions [37]. In Figs. 2(a) and (b) (lower layer), we show the measured average dwell time for 7-step QWs, which are in a good agreement with that from numerical simulations of 7-step QWs (solid curves). The average dwell time of finite-step QWs should approach that of infinite-step QWs (dashed curves) with increas-

ing number of steps [36, 37]. The differences between the experimental results and the simulated ones are due to experimental imperfections, especially decoherence [36].

Topological edge states in non-unitary QWs:— To confirm the non-trivial topological properties of the non-unitary QW, we create regions with distinct topological invariants and probe the existence of edge states via peaked probability distribution at the boundaries for photons still evolving in the QW dynamics. For t -step QWs, such a probability is defined as $Q_{\text{th}}(x, t) = |\langle x | \psi_t \rangle|^2 / |\langle \psi_t | \psi_t \rangle|^2$, which can be experimentally probed by normalized photon counts of the transmitted photons after step t at the position x via a coincidence measurement to the total number of transmitted photons, i.e., $Q_{\text{exp}}(x, t) = N_{\text{T}}(x, t) / \sum_{x'} N_{\text{T}}(x', t)$. The boundaries can be created by making the coin parameters (θ_1, θ_2) spatially inhomogeneous, with $(\theta_1^{(o)}, \theta_2^{(o)})$ in the outer regions ($|x| > x_0$) and $(\theta_1^{(i)}, \theta_2^{(i)})$ in the inner region ($|x| \leq x_0$). These spatially inhomogeneous coin rotations in our experiment are realized via unmounted HWPs individually inserted in specific paths. We choose $x_0 = 4$ in the experiment and fix the coin parameters for the inner region as $(\theta_1^{(i)}, \theta_2^{(i)}) = (\pi/8, 3\pi/16)$, which belong to the topological phase with bulk topological invariants $(\nu_0, \nu_\pi) = (1, -1)$. The walker is initialized at $x = 4$ next to a boundary, and the initial coin state is chosen to be $|+\rangle$ via the delayed-choice setting. For the partial measurement, we fix $p = 2/3$.

First, we choose the coin parameters $(\theta_1^{(o)}, \theta_2^{(o)}) = (\pi/16, \pi/8)$ for the outer regions. As the coins for both the inner and outer regions belong to the same topological phase with $(\nu_0, \nu_\pi) = (1, -1)$, no edge state is ex-

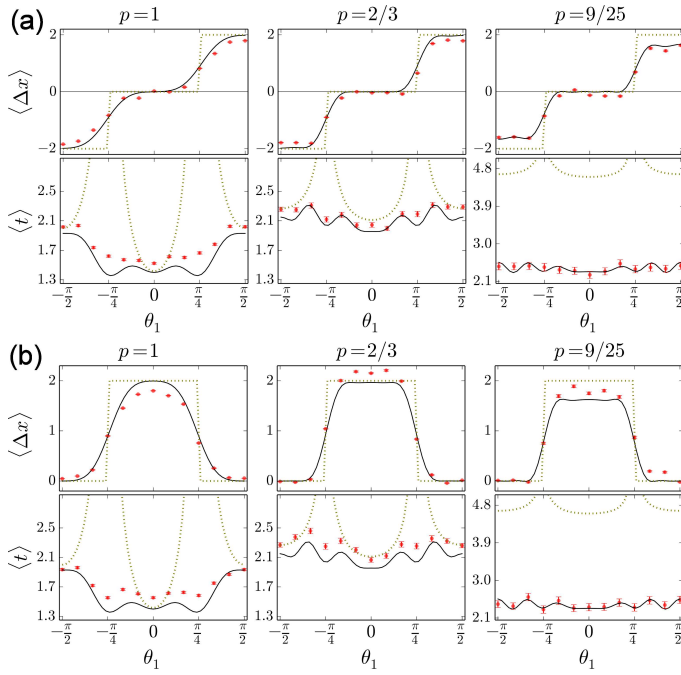


FIG. 2. Measured average displacements (upper layer) and dwell time (lower layer) for 7-step QWs of the protocols \tilde{U}' (a) and \tilde{U}'' (b) as functions of the coin parameter θ_1 ($\theta_2 = \pi/4$ is fixed). The dashed curves indicate the expected results of infinite-step QWs [37]. The solid curves indicate the numerical simulations for 7-step QWs and the experimental results are presented by red dots. Experimental errors are due to photon counting statistics.

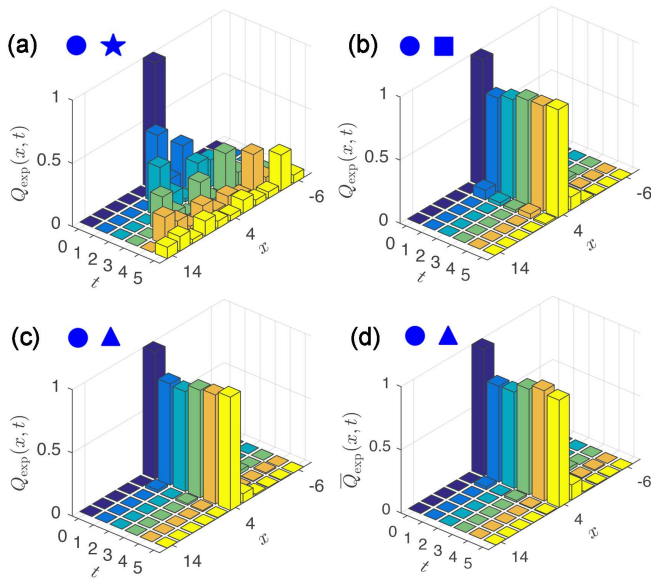


FIG. 3. Experimental observation of topological edge states in 5-step inhomogeneous QWs. (a)-(c) The measured probability distributions $Q_{\text{exp}}(x, t)$ with fixed coin parameters for the inner region and various coin parameters for the outer regions. (d) The experimental results of the mean values of the probabilities of QWs $\bar{Q}_{\text{exp}}(x, t)$ with static disorder introduced to both regions.

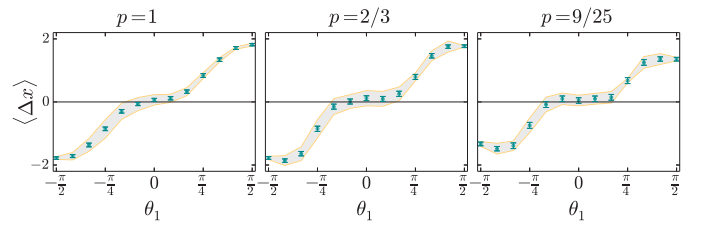


FIG. 4. Average displacements for 5-step QWs with static disordered rotation angles $\theta_{1,2} + \delta\theta$, where $\delta\theta$ is unique for each position and chosen from the intervals $[-\pi/20, \pi/20]$. The coin parameters θ_1 and θ_2 are scanned along the dotted line in Fig. 1(a). The symbols and grey shadings respectively indicate the mean values of the measured average displacements and the range of the standard deviations averaged over 10 different ensembles for each pair (θ_1, θ_2) .

pected. As shown in Fig. 3(a), the distribution up to 5 steps tends to extend with time, and no enhanced probability is observed near the boundary between the inner and outer regions. The wave functions of photons are distributed ballistically, similar to that of the homogenous QW. Here we define the similarity between the measured probability distribution and its theoretical prediction as a figure of merit $S(t) = (\sum_x \sqrt{Q_{\text{exp}}(x, t)Q_{\text{th}}(x, t)})^2$, which ranges between 1 for a perfect match and 0 for a complete mismatch. For the first case, we obtain $S(t=5) = 0.897 \pm 0.018$ [36].

Second, we choose the coin parameters $(-7\pi/16, -3\pi/8)$ for the outer regions, such that these regions belong to the topological phase with $(\nu_0, \nu_\pi) = (-1, -1)$. As the topological invariants ν_0 for the inner and outer regions are different, we expect the existence of topological edge states near the boundary. As shown in Fig. 3(b), the expansion of the wave packet is highly suppressed, and the probability of the photons being detected near the boundary $Q_{\text{exp}}(x=4, t)$ is greatly enhanced, which confirms the existence of localized edge states. The similarity is calculated as $S(t=5) = 0.988 \pm 0.002$, which confirms that the experimentally measured probabilities agree well with the theoretical predictions.

Last, we change the coin parameters for the outer regions to $(-5\pi/8, -9\pi/16)$. Then both topological invariants for the outer regions $(\nu_0, \nu_\pi) = (-1, 1)$ are different from those for the inner region. Our experimental results clearly show the enhanced probability $Q_{\text{exp}}(x=4, t)$ in Fig. 3(c), thus confirming the existence of edge states near the boundary. Here the similarity is $S(t=5) = 0.985 \pm 0.002$.

Robustness against disorder:— A key feature of topologically non-trivial systems is the robustness of the topological properties against small perturbations. We find that both the edge states and the quantization of the average displacement of the non-unitary QW here are robust against static disorder. We first

fix $(\langle\theta_1^{(i)}\rangle, \langle\theta_2^{(i)}\rangle) = (\pi/8, 3\pi/16)$ and $(\langle\theta_1^{(o)}\rangle, \langle\theta_2^{(o)}\rangle) = (-5\pi/8, -9\pi/16)$ for the inner and outer regions, respectively. Static disorder is then introduced to both regions by randomly modulating coin angles within the interval $[\langle\theta_{1,2}^{(i),(o)}\rangle - \pi/20, \langle\theta_{1,2}^{(i),(o)}\rangle + \pi/20]$. The disorder is static in time and independent at each spatial position. We measure $P_{\text{exp}}(x, t')$ ($t' = 1, \dots, 5$) of 5-step QWs with 10 sets of randomly generated coin rotations for each position and calculate the mean values of the probabilities $\overline{Q}_{\text{exp}}(x, t)$. As shown in Fig. 3(d), an enhanced peak in $\overline{Q}_{\text{exp}}(x = 4, t)$ is still observed near the boundary between the regions up to 5 steps, with the similarity in the last step $S(t = 5) = 0.987 \pm 0.001$.

To test the robustness of the quantization of the average displacement against static disorder, we fix the mean value $\langle\theta_2\rangle = \pi/4$ and scan $\langle\theta_1\rangle$ from $-\pi/2$ to $\pi/2$. We then measure $P_{\text{exp}}(x, t')$ ($t' = 1, \dots, 5$) of the 5-step QWs governed by the evolution operator \tilde{U}' with 10 randomly generated coin rotations for each position, and calculate the mean values of the 10 sets of the average displacements. As shown in Fig. 4, the mean values of the average displacements are still quantized, which confirms the robustness of the measurement scheme.

Conclusion.— We have presented the first experimental observation of bulk topological invariants for non-unitary discrete-time QWs. By choosing Floquet operators in different time frames, we are able to detect the two distinct topological invariants for the non-unitary FTP. Our work would stimulate further studies of topological phenomena in non-unitary quantum dynamics in a variety of physical systems.

This work has been supported by the Natural Science Foundation of China (Grant Nos. 11474049, 11674056, 11374283, and 11522545) and the Natural Science Foundation of Jiangsu Province (Grant No. BK20160024). WY acknowledges support from the National Key R&D Program (Grant No. 2016YFA0301700) and the “Strategic Priority Research Program(B)” of the Chinese Academy of Sciences (Grant No. XDB01030200). BCS acknowledges financial support from the 1000-Talent Plan.

* wyiz@ustc.edu.cn

† gnepeux@gmail.com

- [1] M. Z. Hasan and C. L. Kane, “Topological insulators,” *Rev. Mod. Phys.* **82**, 3045–3067 (2010).
- [2] X.-L. Qi and S.-C. Zhang, “Topological insulators and superconductors,” *Rev. Mod. Phys.* **83**, 1057–1110 (2011).
- [3] Z. Wang, Y. Chong, J. D. Joannopoulos, and M. Soljačić, “Observation of unidirectional backscattering-immune topological electromagnetic states,” *Nature* **461**, 772–775 (2009).
- [4] M. C. Rechtsman, J. M. Zeuner, Y. Plotnik, Y. Lumer, D. Podolsky, F. Dreisow, S. Nolte, M. Segev, and A. Szameit, “Photonic Floquet topological insulators,” *Nature* **496**, 196–200 (2013).
- [5] A. B. Khanikaev, S. H. Mousavi, W.-K. Tse, M. Kargarian, A. H. MacDonald, and G. Shvets, “Photonic topological insulators,” *Nat. Mater.* **12**, 233–239 (2013).
- [6] M. Hafezi, S. Mittal, J. Fan, A. Migdall, and J. M. Taylor, “Imaging topological edge states in silicon photonics,” *Nat. Photonics* **7**, 1001–1005 (2013).
- [7] L. Lu, J. D. Joannopoulos, and M. Soljačić, “Topological photonics,” *Nat. Photonics* **8**, 821–829 (2014).
- [8] X. Cheng, C. Jouvaud, X. Ni, S. H. Mousavi, A. Z. Genack, and A. B. Khanikaev, “Robust reconfigurable electromagnetic pathways within a photonic topological insulator,” *Nat. Mater.* **15**, 542 (2016).
- [9] F. Cardano, M. Maffei, F. Massa, B. Piccirillo, C. De Lisio, G. De Filippis, V. Cataudella, E. Santamato, and L. Marrucci, “Statistical moments of quantum-walk dynamics reveal topological quantum transitions,” *Nat. Commun.* **7**, 11439 (2016).
- [10] S. Barkhofen, T. Nitsche, F. Elster, L. Lorz, A. Gabris, I. Jex, and C. Silberhorn, “Measuring topological invariants and protected bound states in disordered discrete time quantum walks,” arXiv:1606.00299.
- [11] F. Cardano, A. D’Errico, A. Dauphin, M. Maffei, B. Piccirillo, C. de Lisio, G. De Filippis, V. Cataudella, E. Santamato, L. Marrucci, M. Lewenstein, and P. Massignan, “Detection of Zak phases and topological invariants in a chiral quantum walk of twisted photons,” *Nat. Commun.* **8**, 15516 (2017).
- [12] J. M. Zeuner, M. C. Rechtsman, Y. Plotnik, Y. Lumer, S. Nolte, M. S. S. Rudner, M. Segev, and A. Szameit, “Observation of a topological transition in the bulk of a non-Hermitian system,” *Phys. Rev. Lett.* **115**, 040402 (2015).
- [13] S. Weimann, M. Kremer, Y. Plotnik, Y. Lumer, S. Nolte, K. G. Makris, M. Segev, M. C. Rechtsman, and A. Szameit, “Topologically protected bound states in photonic parity-time-symmetric crystals,” *Nat. Mater.* **16**, 433–438 (2017).
- [14] M. Bellec, U. Kuhl, G. Montambaux, and F. Mortessagne, “Topological transition of Dirac points in a microwave experiment,” *Phys. Rev. Lett.* **110**, 033902 (2013).
- [15] C. Poli, M. Bellec, U. Kuhl, F. Mortessagne, and H. Schomerus, “Selective enhancement of topologically induced interface states in a dielectric resonator chain,” *Nat. Commun.* **6**, 6710 (2015).
- [16] W. Hu, J. C. Pillay, K. Wu, M. Pasek, P. P. Shum, and Y. D. Chong, “Measurement of a topological edge invariant in a microwave network,” *Phys. Rev. X* **5**, 011012 (2015).
- [17] R. Süsstrunk and S. D. Huber, “Observation of phononic helical edge states in a mechanical topological insulator,” *Science* **349**, 47–50 (2015).
- [18] R. Fleury, A. B. Khanikaev, and A. Alù, “Floquet topological insulators for sound,” *Nat. Commun.* **7**, 11744 (2016).
- [19] M. Atala, M. Aidelsburger, J. T. Barreiro, D. Abanin, T. Kitagawa, E. Demler, and I. Bloch, “Direct measurement of the Zak phase in topological Bloch bands,” *Nat. Phys.* **9**, 795–800 (2013).
- [20] G. Jotzu, M. Messer, R. Desbuquois, M. Lebrat, T. Uehlinger, D. Greif, and T. Esslinger, “Experimental realization of the topological Haldane model with ultra-

- cold fermions,” *Nature* **515**, 237–240 (2014).
- [21] M. Aidelsburger, M. Lohse, C. Schweizer, M. Atala, J. T. Barreiro, S. Nascimbene, N. R. Cooper, I. Bloch, and N. Goldman, “Measuring the Chern number of Hofstadter bands with ultracold bosonic atoms,” *Nat. Phys.* **11**, 162–166 (2015).
- [22] N. Fläschner, B. S. Rem, M. Tarnowski, D. Vogel, D.-S. Lühmann, K. Sengstock, and C. Weitenberg, “Experimental reconstruction of the Berry curvature in a Floquet Bloch band,” *Science* **352**, 1091–1094 (2016).
- [23] T. Li, L. Duca, M. Reitter, F. Grusdt, E. Demler, M. Endres, M. Schleier-Smith, I. Bloch, and U. Schneider, “Bloch state tomography using Wilson lines,” *Science* **352**, 1094–1097 (2016).
- [24] M. Leder, C. Grossert, L. Sitta, M. Genske, A. Rosch, and M. Weitz, “Real-space imaging of a topologically protected edge state with ultracold atoms in an amplitude-chirped optical lattice,” *Nat. Commun.* **7**, 13112 (2016).
- [25] E. J. Meier, F. A. An, and B. Gadway, “Observation of the topological soliton state in the Su–Schrieffer–Heeger model,” *Nat. Commun.* **7**, 13986 (2016).
- [26] T. Kitagawa, M. A. Broome, A. Fedrizzi, M. S. Rudner, E. Berg, I. Kassal, A. Aspuru-Guzik, E. Demler, and A. G. White, “Observation of topologically protected bound states in photonic quantum walks,” *Nat. Commun.* **3**, 882 (2012).
- [27] S. Ryu, A. P. Schnyder, A. Furusaki, and A. W. W. Ludwig, “Topological insulators and superconductors: tenfold way and dimensional hierarchy,” *New J. Phys.* **12**, 065010 (2010).
- [28] J. C. Y. Teo and C. L. Kane, “Topological defects and gapless modes in insulators and superconductors,” *Phys. Rev. B* **82**, 115120 (2010).
- [29] V. V. Ramasesh, E. Flurin, M. Rudner, I. Siddiqi, and N. Y. Yao, “Direct probe of topological invariants using Bloch oscillating quantum walks,” *Phys. Rev. Lett.* **118**, 130501 (2017).
- [30] E. Flurin, V. V. Ramasesh, S. Hacoheh-Gourgy, L. S. Martin, N. Y. Yao, and I. Siddiqi, “Observing topological invariants using quantum walks in superconducting circuits,” *Phys. Rev. X* **7**, 031023 (2017).
- [31] M. S. Rudner and L. S. Levitov, “Topological transition in a non-Hermitian quantum walk,” *Phys. Rev. Lett.* **102**, 065703 (2009).
- [32] M. S. Rudner, M. Levin, and L. S. Levitov, “Survival, decay, and topological protection in non-Hermitian quantum transport,” arXiv:1605.07652 (2016).
- [33] K. Esaki, M. Sato, K. Hasebe, and M. Kohmoto, “Edge states and topological phases in non-Hermitian systems,” *Phys. Rev. B* **84**, 205128 (2011).
- [34] D. Kim, M. Ken, N. Kawakami, and H. Obuse, “Floquet topological phases driven by \mathcal{PT} symmetric nonunitary time evolution,” arXiv:1609.09650 (2016).
- [35] Y.-C. Jeong, C. Di Franco, H.-T. Lim, M. S. Kim, and Y.-H. Kim, “Experimental realization of a delayed-choice quantum walk,” *Nat. Commun.* **4**, 2471 (2013).
- [36] See the Supplemental Material at <http://link.aps.org/supplemental/10.1103/PhysRevLett.119.130501> for details on the derivation of the topological invariants of the nonunitary discrete-time QW, the application of the delayed-choice QW, the convergence of average dwell time, the robustness of the topological properties of the QW and the measurement scheme of the topological invariants against dynamic disorder, and the impact of decoherence on the experimental measurements.
- [37] T. Rakovszky, J. K. Asbóth, and A. Alberti, “Detecting topological invariants in chiral symmetric insulators via losses,” *Phys. Rev. B* **95**, 201407 (2017).
- [38] L. Jiang, T. Kitagawa, J. Alicea, A. R. Akhmerov, D. Pekker, G. Refael, J. I. Cirac, E. Demler, M. D. Lukin, and P. Zoller, “Majorana fermions in equilibrium and in driven cold-atom quantum wires,” *Phys. Rev. Lett.* **106**, 220402 (2011).
- [39] J. K. Asbóth, “Symmetries, topological phases, and bound states in the one-dimensional quantum walk,” *Phys. Rev. B* **86**, 195414 (2012).
- [40] J. K. Asbóth and H. Obuse, “Bulk-boundary correspondence for chiral symmetric quantum walks,” *Phys. Rev. B* **88**, 121406 (2013).
- [41] T. Kitagawa, M. S. Rudner, E. Berg, and E. Demler, “Exploring topological phases with quantum walks,” *Phys. Rev. A* **82**, 033429 (2010).
- [42] M. A. Broome, A. Fedrizzi, B. P. Lanyon, I. Kassal, A. Aspuru-Guzik, and A. G. White, “Discrete single-photon quantum walks with tunable decoherence,” *Phys. Rev. Lett.* **104**, 153602 (2010).